nature portfolio

https://doi.org/10.1038/s41558-022-01353-1

Supplementary information

Trophic level decoupling drives future changes in phytoplankton bloom phenology

In the format provided by the authors and unedited

Supplementary information for
Trophic level decoupling drives future changes in phytoplankton bloom phenology

Ryohei Yamaguchi[1,2 *], Keith B Rodgers[1,2], Axel Timmermann[1,2], Karl J Stein[1,2], Sarah Schlunegger[3], Daniele Bianchi[4], John P Dunne[5], and Richard Slater[3]

[1] *Center for Climate Physics, Institute for Basic Science, Busan, South Korea*

[2] *Pusan National University, Busan, South Korea*

[3] *AOS Program, Princeton University, NJ, United States*

[4] *Department of Atmospheric and Oceanic Sciences, University of California, Los Angeles, CA, United States*

[5] *NOAA/OAR Geophysical Fluid Dynamics Laboratory, NJ, United States*

***** Corresponding author: Ryohei Yamaguchi (ryamaguchi@pusan.ac.kr)

Contents

Note 1. Model-Observation comparison of seasonal cycle of sea surface chlorophyll

Results of a comparison of phytoplankton phenology between ESM2M and observational data are summarized in Figure. S1–S4, and Extended Data Figure 1.

We first present biome-averaged normalized seasonal cycles of sea surface chlorophyll (Chl) to compare ESM2M and observations focusing on the phase of the seasonal cycle (Fig. S1), namely the main focus of this study. The analysis reveals that the model reproduces the observed phase of the seasonal cycle of phytoplankton relatively well, but that there are some limited regions where the model simulation is less satisfactory, especially in the high latitudes of the Southern Hemisphere (SI_SPSS, SA_SPSS, SP_SPSS, S_ICE) and the northern Indian Ocean (NI_STPS). Correlation coefficients of the daily climatology of the modeled and observed seasonal cycles also are small in these ocean regions (Fig. S2). An important source of these biases might be in large part due to biases in the simulated seasonal cycle for the physical state of the model. The overly intense summer stratification bias and associated warm sea surface temperature in the Southern Ocean in this model (Dunne et al., 2012[1]) can lead to anomalous accumulation of biomass in the sub-surface layer and can induce the apparent autumn bloom when the mixed layer (ML) deepens, as seen in Figure S1r, S1s, and S1t.

While there are such phase biases in the seasonal cycle of Chl considered as a biome-mean, the model captures well the spatial structure of both phytoplankton bloom phase and amplitude characteristics (Fig. S3). In the Northern Hemisphere, the model reproduces the observed meridional structure of a gradual delay in bloom peak and initiation as latitude increases from the mid- to high-latitudes. In the Southern Hemisphere, the model shows spatial patterns that are similar as the observations, with relatively uniform bloom peak timing in the mid-latitude oceans, and with a marked transition to the Antarctic circumpolar current region. However, as seen in Figure S1, there is an overall early bias in the circumpolar current region.

The relative standard deviations in Figure S2 provide us with information about the model-observation difference in the amplitude of the seasonal cycle in Chl. As the standard deviation in Figure S2 is normalized by the corresponding observations in each biome, the closer the value is to unity (dotted line in the figure), the better the model represents the observed amplitude of the seasonal cycle. In the STSS of the South Pacific and South Indian Ocean, the modeled seasonal amplitude is almost three times larger than that in the observations. The model tends to underestimate the magnitude of the phytoplankton bloom in coastal regions, and slightly overestimates the magnitude in the open ocean, although the model reproduces well the overall spatial pattern (Fig. S3e, and S3f). This is undoubtedly largely due to the fact that the model used in this study has low-resolution and does not reproduce the small spatial-scale coastal processes, such as coastal-open ocean water exchange and atmospheric deposition of terrestrial-origin materials.

Extended Data Figure 1 demonstrates that, in a biome mean sense, the ensemble spread of the 30-member ESM2M Large Ensemble successfully reproduces the magnitude of the natural variability in the observed features of bloom phenology. On the other hand, model underestimates observed natural variability in bloom magnitude in many biomes (Fig. S4). This as may as well be a consequence of low-resolution models not being able to reproduce processes with small spatiotemporal scales that can drive extreme phytoplankton variability. As the Time of Emergence (ToE, Methods) in this study is estimated using the ratio of the forced trend (ensemble mean, signal) to the background natural variability (ensemble standard deviation, noise), this gives us a degree of confidence that the ToE estimated by using future projections with ESM2M is relatively reliable for phenological aspects of the phytoplankton bloom (initiation and peak timing), but it should be noted that the ToE for the bloom magnitude may be underestimated.

A comparison of the interannual variability in the phytoplankton bloom phenological features and magnitude in each biome is shown in Extended Data Figure 1 and Figure S4. This analysis reveals that both phenological and magnitude features have large internal variability in observations, and that the observational records are still too short to detect the forced (anthropogenic) long-term trend.

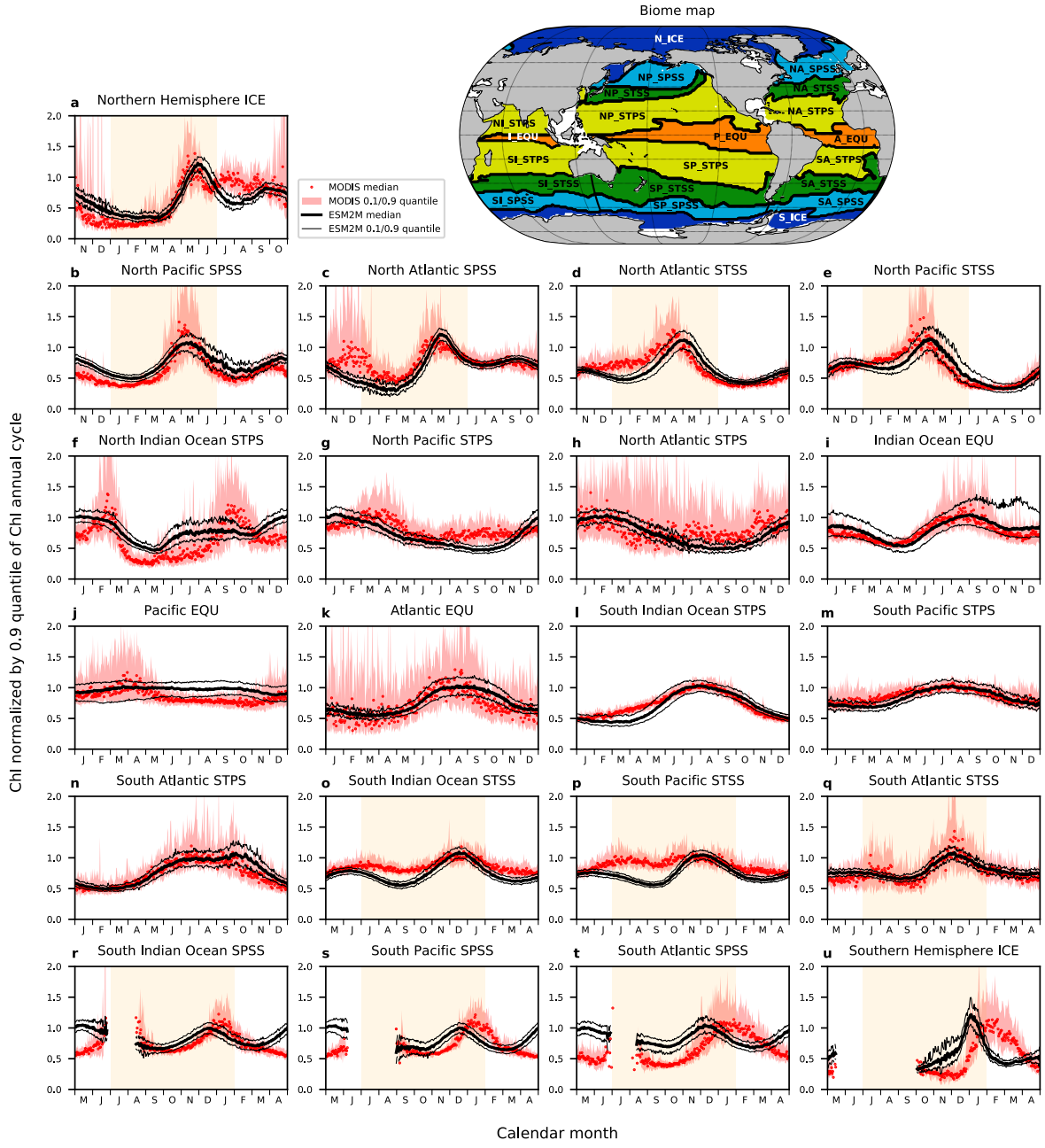

Fig. S1 | Biome map and normalized climatological annual cycle of surface chlorophyll concentrations from satellite observations (MODIS Aqua) and from the ESM2M Large Ensemble simulations. For the observational time series (red), median and 0.1/0.9 quantile values of a 17 years record (2003-2019) are calculated at each day of the year. For model time series (black), after resampling that uses information based on missing data in observational records, median and 0.1/0.9 quantile values of 17 years times 30 ensemble members are calculated. To compare the observations and the model by focusing on phase rather than amplitude, the time series is normalized by the 0.9 quantile value of each annual cycle. It should be noted that the x-axis is shifted so that the spring in each hemisphere is located in the middle of the panels. The period shaded in light orange is the period during which the bloom is recognized as a spring bloom in this study.

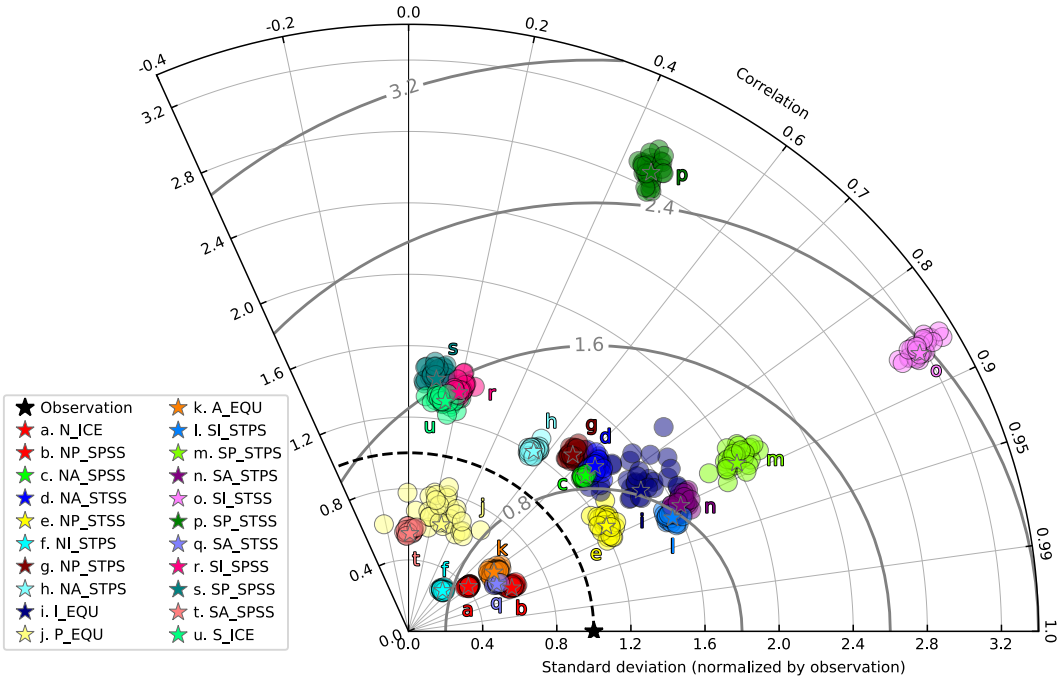

Fig. S2 | ESM2M skill in reproducing the climatological (2003-2019 mean) annual cycle of surface chlorophyll concentrations from remote-sensing products. Correlation between ESM2M's annual cycle and the observed annual cycle, standard deviation of ESM2M's annual cycle relative to standard deviation of the observed seasonal cycle ($\sigma_{\mathrm{ESM2M}}/\sigma_{\mathrm{Obs}}$), and root-mean-square difference between ESM2M's annual cycle and the observed annual cycle divided by the standard deviation of the observed seasonal cycle (RMSD/ σ_{Obs}) are represented as the azimuthal angle, the radial distance from the origin, and the distance from the point on the x-axis labeled as observations (black star), respectively. After resampling the model data based on missing data information in observational records, these three metrics are calculated from both individual members (circles) and ensemble median (stars) for each biome.

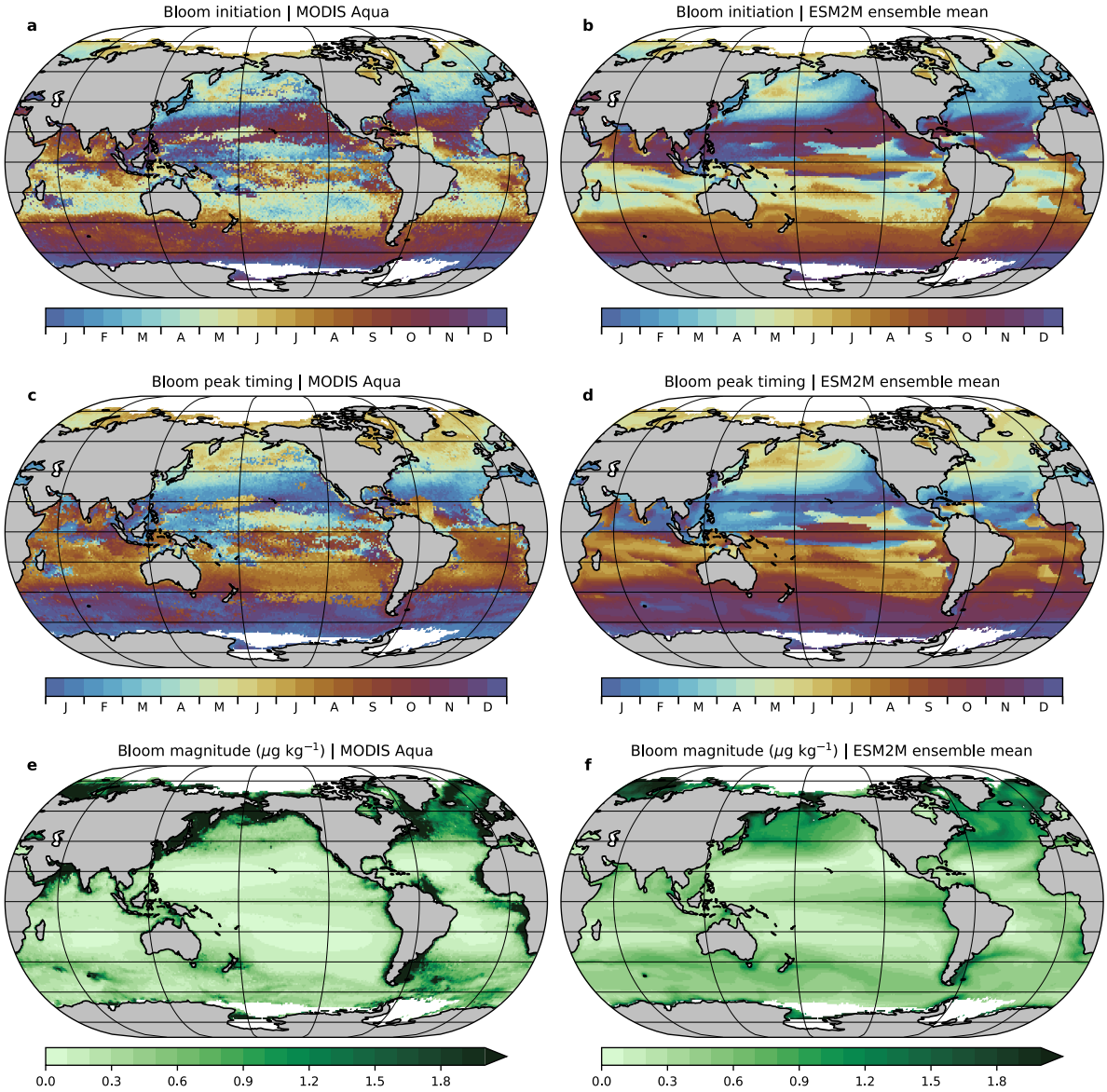

Fig. S3 | Climatological mean (2003-2019) phytoplankton bloom timing (initiation and peak, [calendar month]) and magnitude [mg m^{-3}] from remote sensing products (MODIS Aqua) and from the ESM2M large ensemble simulations. The bloom initiation and peak timing are defined based on phytoplankton accumulation rates ($r \equiv \frac{d\ln(Chl)}{dt}$), and the magnitude is the surface chlorophyll concentration at the timing of the bloom peak (see Methods). In this comparison, individual ensemble members are resampled by removing output corresponding to spatiotemporal coordinates of missing data from the observational record, and subsequently the timing and magnitude are estimated for each member.

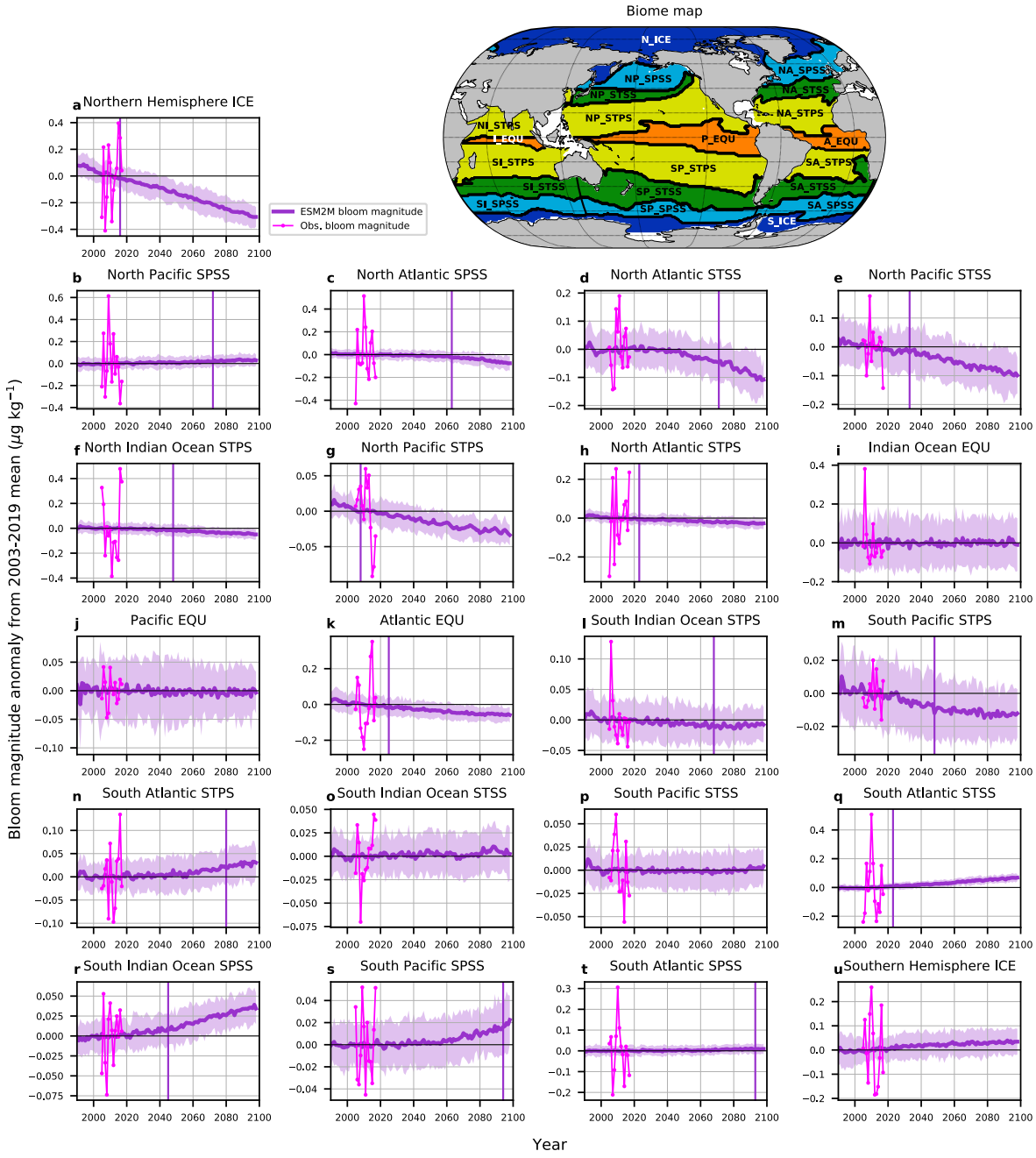

Fig. S4 | Biome-aggregated observational and ESM2M time series of bloom magnitude anomalies relative to the satellite observational period means (2003-2019). The shadings on the lines represent the two standard deviation range of the 30 ensemble members of ESM2M. Time of emergence (ToE) of the biome-aggregated changes in the bloom magnitude are shown in the vertical lines. For the case where there is no corresponding vertical line in the panel, the magnitude change will not be emergent by the end of simulation period. It should be noted that the model time series are created without the resampling process in order to be consistent along the time-dimension of the model output from year 1990 to the end of the simulation (year 2100).

Note 2. Computing the accumulation rate budget from monthly output

Following the formulations of the biogeochemical component of GFDL-ESM2M (TOPAZ2; Dunne et al., 2013[2]), we calculated terms in the accumulation rate budget equation separately for three phytoplankton groups from monthly model outputs. In TOPAZ2, phytoplankton biomass is prognostically computed based on nitrogen. As the phytoplanktonic nitrogen is instantly converted to carbon units using a fixed organic C:N ratio (106:16), we employ the more widely used terminology of the chlorophyll to carbon ratio (θ), instead of the nitrogen-chlorophyll ratio.

When using temperature and nutrient concentration fields, the temperature limitation and nutrient limitation for phytoplankton growth are calculated as follows:

$$T^{lim} = e^{0.063T}, \tag{S1}$$

$$\begin{aligned} N_{Sp}^{lim} &= \mathrm{Min}\left(Lim_{Sp}^{NO_3} + Lim_{Sp}^{NH_4}, Def_{Sp}^{PO_4}, Def_{Sp}^{Fe}\right), \\ N_{Lg}^{lim} &= \mathrm{Min}\left(Lim_{Lg}^{NO_3} + Lim_{Lg}^{NH_4}, Def_{Lg}^{PO_4}, Def_{Lg}^{Fe}\right), \\ N_{Di}^{lim} &= \mathrm{Min}\left(Def_{Di}^{PO_4}, Def_{Di}^{Fe}\right), \end{aligned} \tag{S2}$$

where $Lim_i^{NO_3}$, $Lim_i^{NH_4}$, Def_i^P, and $,Def_i^{Fe}$ represent limitations and deficiencies of individual nutrients (Nitrate, ammonia, phosphate, and iron) which are parametrized based on uptake velocities, and subscription i indicates phytoplankton groups ($i = Sp, Lg, and\ Di$ for small, large, and diazotrophic phytoplankton). The nutrient- and temperature-limited growth rates for three phytoplankton groups are

$$P_i^{cm} = P_i^{cmax} N_i^{lim} T^{lim}, \tag{S3}$$

where P_i^{cmax} are constants of the maximum growth rate given by Geider et al. (1997)[3]. The chlorophyll-carbon ratio is calculated using the nutrient and temperature limited growth rate and irradiance averaged over the KPP boundary layer with 24-hr memory (IRR_{mem}),

$$\theta_i = \theta_i^{min} + \frac{\theta_i^{max} - \theta_i^{min}}{1 + (\theta_i^{max} - \theta_i^{min}) \frac{\alpha_i I R R_{mem}}{2 P_i^{cm}}}, \quad \text{(S4)}$$

where θ_i^{min} is a function of nutrient limitation (N_i^{lim}), and θ_i^{max} and α_i are given constants for the three phytoplankton groups. Although chlorophyll concentrations are also available from standard model output, we can reconstruct chlorophyll concentrations from the calculated chlorophyll-carbon ratio to check whether the above calculations are valid,

$$Chl_i = \left(\frac{106}{16}\right) \theta_i P_i. \quad \text{(S5)}$$

The light limitation for phytoplankton is modeled after Geider et al. (1997)[3] with some modifications by Dunne et al. (2013b)[2],

$$L_i^{lim} = 1 - e^{-\frac{\alpha_i \theta_i I R R}{P_i^{cm}}}. \quad \text{(S6)}$$

And the phytoplankton growth rate is given as

$$\mu_i = \frac{P_i^{cm} L_i^{lim}}{1+\zeta} = \frac{P_i^{cmax}}{1+\zeta} T^{lim} N_i^{lim} L_i^{lim}. \quad \text{(S7)}$$

On the other hand, the phytoplankton loss rate is parameterized as a function of temperature and phytoplankton biomass concentrations:

$$\begin{aligned} l_{Sp} &= \text{Min}\left(\frac{1}{\Delta t}, \frac{\lambda_0 T^{lim} P_{Sp}^2}{P^* (P_{Sp} + P^{min})}\right), \\ l_{Lg} &= \text{Min}\left(\frac{1}{\Delta t}, graze * P_{Lg}\right), \\ l_{Di} &= \text{Min}\left(\frac{1}{\Delta t}, graze * P_{Di}\right), \\ graze &= \frac{\lambda_0 T^{lim} \left(\frac{P_{Lg}+P_{Di}}{P^*}\right)^{\frac{1}{3}} \left(\frac{P_{Lg}+P_{Di}}{P_{Lg}+P_{Di}+P^{min}}\right)}{\left(P_{Lg}^2 + P_{Di}^2\right)^{\frac{1}{2}}}. \end{aligned} \quad \text{(S8)}$$

Although this parametrization for the phytoplankton loss doesn't include some well-known processes that have confirmed from observations and laboratory experiments (e.g., viral lysis), the phytoplankton concentration-based parametrization of the loss rate by grazing (proportional to concentration to the 2nd and 4/3rd power for small/diazotrophic plankton and

large phytoplankton, respectively) can allow to represent tight coupling between phytoplankton growth and predation by zooplankton[4], as seen in recent observational records. Therefore, net accumulation by decrease in the loss rate due to the phytoplankton concentration change (e.g., by deepening of the mixed layer) can happen in the model even without increase in the growth rate.

Using Equations S4, S7, and S8 with ML depth (h), the accumulation rate budget equation (Equation 1 in Main text and Eq. M2 in Methods) can be obtained:

$$\begin{aligned} \frac{d\ln(Chl)}{dt} \equiv r &\approx \sum_{i=1}^{3}\left((\mu_i - l_i) + \frac{d\ln(\theta_i)}{dt}\right)\gamma_i - \frac{d\ln(h)}{dt} \\ &\equiv \mu - l + \frac{d\ln(\theta)}{dt} - \frac{d\ln(h)}{dt} \end{aligned} \quad \text{(S9)}$$

where Chl is sum of chlorophyll concentrations of three groups ($chl = \sum_{i=1}^{3} Chl_i$), and γ_i represents the concentration ratio for each group ($\gamma_i = Chl_i/Chl$). In this analysis, to avoid overestimation of the light limitation term due to using monthly outputs of irradiance fields, we first calculated the growth rate as the residual of the accumulation rate budget equation (Equation S9), and then estimated the light limitation term from the estimated growth rate and nutrient- and temperature-limitation terms (Equation S7).

Table 1 | List of variables and constants in Note 2

Symbol	Name	Unit
P_i	Phytoplankton biomass	mol N kg^{-1}
θ_i	Chlorophyll to Carbon ratio	g Chl g C^{-1}
θ_i^{min}, θ_i^{max}	Minimum/Maximum θ_i	g Chl g C^{-1}
T^{lim}	Temperature limitation	Dimensionless
L_i^{lim}	Light limitation	Dimensionless
N_i^{lim}	Nutrient limitation	Dimensionless
P_i^{cm}	Nutrient- and Temperature-limited growth rate	s^{-1}
P_i^{cmax}	Maximum P_i^{cm}	s^{-1}
$Lim_i^{NO_3}, Lim_i^{NH_4}$	Nitrate/Ammonium limitation	Dimensionless
$Def_i^{PO_4}, Def_i^{PO_4}$	Phosphorus/Iron deficiency	Dimensionless
IRR	Irradiance	W m^{-2}
IRR_{mem}	Irradiance averaged over the KPP boundary layer with 24-hr memory	W m^{-2}
α_i	Light harvest coefficient	gC $gChl^{-1}$ m^2 W^{-1} s^{-1}
μ_i	Phytoplankton growth rate	s^{-1}
l_i	Phytoplankton loss rate	s^{-1}
ζ	Photorespiration loss (0.1)	Dimensionless
λ_0	Grazing rate constant at 0ºC	s^{-1}
P^{min}	Minimum phytoplankton concentration threshold for grazing	mol N kg^{-1}
P^*	Pivot phytoplankton concentration for grazing allometry	mol N kg^{-}

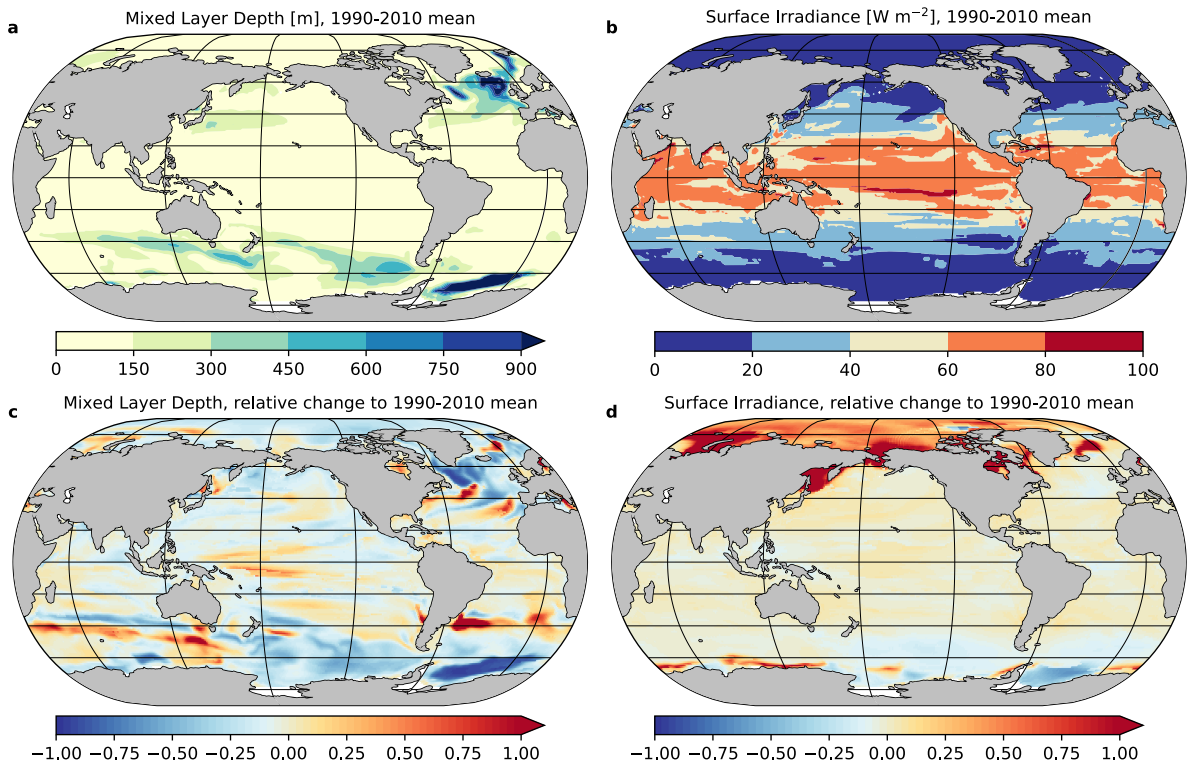

Fig. S5 | Climatologies and future changes in the environmental drivers regulating the light limitation for phytoplankton growth at timing of bloom initiation. Present-day (1990–2010) mean (a) mixed layer depth and (b) sea surface irradiance and relative change in (c) mixed later depth and (d) sea surface irradiance from present day to future (2080–2100) periods in the month of bloom initiation (c.f., Fig. 1a). The changes are values relative to present day mean fields, or equivalently, divided by present day means.

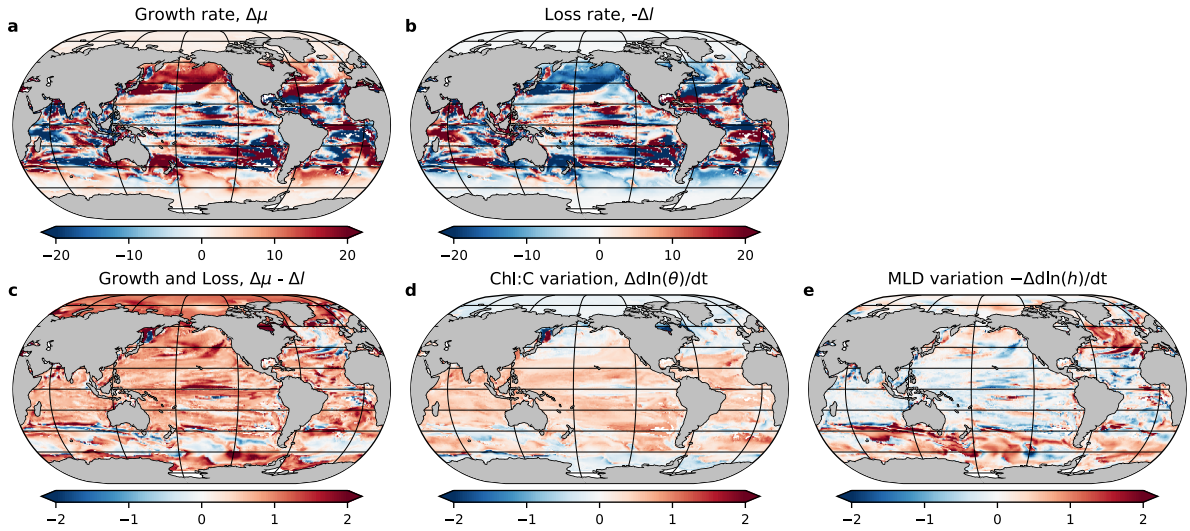

Fig. S6 | Relative contributions in the accumulation rate budget analysis to shift in timing of the bloom initiation. In addition to relative contributions from phytoplankton growth rate and loss rate change individually, relative contributions of the three driving processes (decoupling between changes in growth and loss rate; $\Delta\mu - \Delta l$, change in temporal variation in mixed layer depth (MLD); $-\Delta\, d\ln h/dt$, and change in Chl:C variation; $\Delta\, d\ln\theta/dt$) are shown. Relative contributions are the ratio of (1) the time-integrated RHS terms of Equation M5 over the period between bloom peak timing for the present day and the future to (2) the term on the LHS (Equation M6).

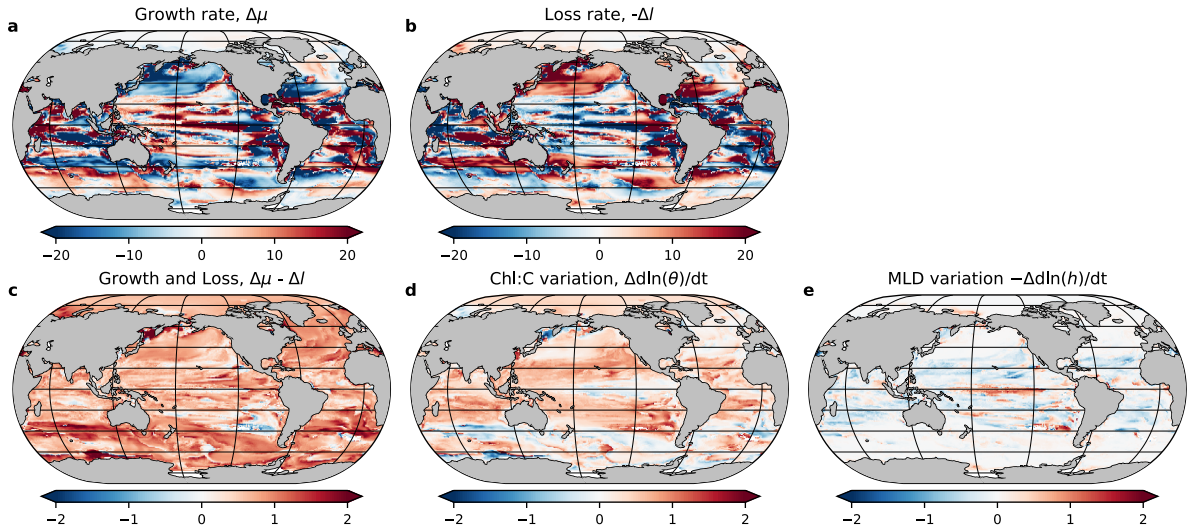

Fig. S7 | Relative contributions in the accumulation rate budget analysis to shift in timing of the bloom peak. Same as Fig. S6, but for bloom peak timing.

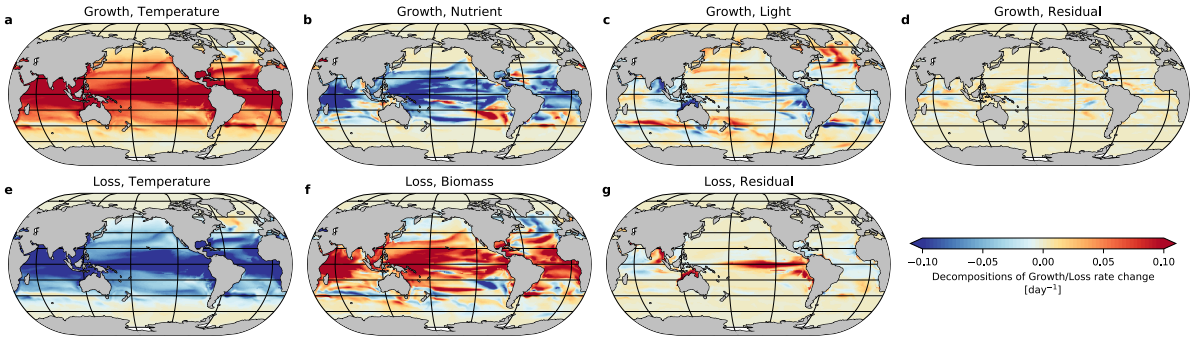

Fig. S8 | Decomposition of future changes in time-integrated growth and loss rate over the period between future and present-day bloom initiation. Growth rate change ($\Delta\mu$) and loss rate change ($-\Delta l$) can be decomposed into temperature-, nutrient-, and light-limitation terms, and temperature-limitation and biomass terms, respectively (Equations M7 and M8).

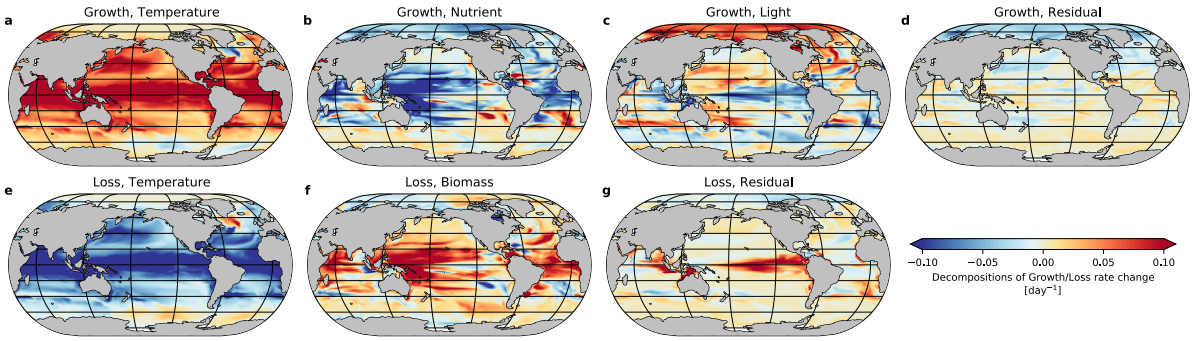

Fig. S9 | Decomposition of future changes in time-integrated growth and loss rate over the period between future and present-day bloom peak timing. Same as Fig. S8, but for bloom peak timing.

References

1. Dunne, J. P. *et al.* GFDL's ESM2 Global Coupled Climate–Carbon Earth System Models. Part I: Physical Formulation and Baseline Simulation Characteristics. *Journal of Climate* **25**, 6646–6665 (2012).
2. Dunne, J. P. *et al.* GFDL's ESM2 Global Coupled Climate–Carbon Earth System Models. Part II: Carbon System Formulation and Baseline Simulation Characteristics*. *Journal of Climate* **26**, 2247–2267 (2013).
3. Geider, R., MacIntyre, H. & Kana, T. Dynamic model of phytoplankton growth and acclimation:responses of the balanced growth rate and the chlorophyll a:carbon ratio to light, nutrient-limitation and temperature. *Mar. Ecol. Prog. Ser.* **148**, 187–200 (1997).
4. Freilich, M., Mignot, A., Flierl, G. & Ferrari, R. Grazing behavior and winter phytoplankton accumulation. *Biogeosciences* **18**, 5595–5607 (2021).